Pharmacological Research 169 (2021) 105660

Contents lists available at ScienceDirect

Pharmacological Research

journal homepage: www.elsevier.com/locate/yphrs

Invited Review

Hydrophobic and polar interactions of FDA-approved small molecule protein kinase inhibitors with their target enzymes

Robert Roskoski Jr

Blue Ridge Institute for Medical Research, 3754 Brevard Road, Suite 116, Box 19, Horse Shoe, NC 28742-8814, United States

ARTICLE INFO

Keywords:
Catalytic spine
KLIFS residues
Protein kinase inhibitor classification
Protein kinase structure
Regulatory spine
Targeted cancer therapy

Chemical compounds studied in this article:
Afatinib (PubChem CID: 10184653)
Cobimetinib (PubChem CID: 16222096)
Crizotinib (PubChem CID: 11626560)
Gefitinib (PubChem CID: 123631)
Imatinib (PubChem CID: 5291)
Ibrutinib (PubChem CID: 24821094)
Selumetinib (PubChem CID: 10127622)
Sorafenib (PubChem CID: 216239)
Sunitinib (PubChem CID: 5329102)
Tofacitinib (PubChem CID: 9926791)

ABSTRACT

Dysregulation and mutations of protein kinases play causal roles in many diseases including cancer. The KLIFS (kinase–ligand interaction fingerprint and structure) catalog includes 85 ligand binding-site residues occurring in both the small and large protein kinase lobes. Except for allosteric inhibitors, all FDA-approved drug-target enzyme complexes display hydrophobic interactions involving catalytic spine residue-6 (KLIFS-77), catalytic spine residue-7 (KLIFS-11), and catalytic spine residue-8 (KLIFS-15) within the small lobe and residues within the hinge-linker region (KLIFS-46–52). Except for allosteric antagonists, the approved drugs form hydrogen bonds with the third hinge residue (KLIFS-48) of their target. Most of the approved drugs, including the allosteric inhibitors, interact with the small lobe gatekeeper residue (KLIFS-45). The type IIA inhibitors have the most hydrophobic interactions with their target enzymes. These include interactions with KLIFS-27/31/35/61/66 residues of the back pocket within both the small and large lobes. There is also interaction with KLIFS-68 (regulatory spine residue-1), the conserved histidine of the catalytic loop that is found in the back pocket of type II antagonists, but within the front pocket of the other types of inhibitors. Owing to the participation of protein kinase signaling cascades in a wide variety of physiological and pathological processes, one can foresee the increasing use of targeted inhibitors both as primary and secondary treatments for many illnesses. Further studies of protein kinase signal transduction pathways promise to yield new and actionable information that will serve as a basis for fundamental and applied biomedical breakthroughs.

1. Overviews of protein kinase structures and mechanism

Eukaryotic protein kinases (ePKs) play crucial roles in nearly every aspect of cell biology [1–4]. These enzymes regulate metabolism, transcription, translation, macromolecule biosynthesis, cell growth, cell division, cell migration, and the immune response. Phosphorylation-dephosphorylation is an overall reversible process that involves the participation of both protein kinases and phosphoprotein phosphatases. Dysregulation of protein kinase signaling pathways occurs in many diseases including autoimmune, inflammatory, and nervous system disorders, cancer, and diabetes. Both academic and commercial investigators have performed studies to determine the physiological and pathological functions of protein-kinase signal transduction pathways during the past 50 years.

Protein kinases catalyze the following reaction:

$$MgATP^{1-} + \text{protein–O:H} \rightarrow \text{protein–O:}PO_3^{2-} + MgADP + H^+$$

This equation indicates that the phosphorylium ion (PO_3^{2-}), and not the phosphate group (OPO_3^{2-}) is transferred from ATP to the protein substrate. Based upon the identity of the phosphorylated –OH group, these catalysts are classified as protein-serine/threonine or protein-tyrosine kinases [5]. A small group of dual-specificity protein kinases including MEK1 and MEK2 catalyzes the phosphorylation of ERK1 and ERK2 at tyrosine before threonine in the ERK activation segment sequence consisting of Thr-Glu-Tyr [6,7]. These dual-specificity protein kinases are members of the protein-serine/threonine kinase family.

The catalytic domain of generic protein kinases consists of about 250 amino acid residues [8]. The catalytic domain of various protein kinases varies considerably owing to one or more kinase domain insertions.

Abbreviations: aPK, atypical protein kinase; AS, activation segment; BTK, Bruton protein-tyrosine kinase; CS or C-spine, catalytic spine; CL, catalytic loop; EGFR, epidermal growth factor receptor; ePK, eukaryotic protein kinase; GK, gatekeeper; GRL, Gly-rich loop; NSCLC, non-small cell lung cancer; PDGFR, platelet-derived growth factor receptor; PKA, protein kinase A; PKC, protein kinase C; RS or R-spine, regulatory spine; Sh2, shell residue 2; VEGFR, vascular endothelial growth factor receptor.

E-mail address: rrj@brimr.org.

https://doi.org/10.1016/j.phrs.2021.105660
Received 30 April 2021; Accepted 30 April 2021
Available online 7 May 2021

Based upon the primary structures of about five dozen protein-serine/threonine and protein-tyrosine kinases, Hanks and Hunter subdivided them into 12 domains (I-VIA, VIB-XI) [9]. Protein kinase domain I contains a glycine-rich loop (GRL) with a GxGxΦG signature, where Φ refers to a hydrophobic residue such as phenylalanine. The glycine-rich loop connects the β1- and β2-strands of the small amino-terminal lobe that make up the roof of the ATP/ADP-binding site. This flexible glycine-rich loop facilitates both ATP binding and ADP release during each reaction cycle. Protein kinase domain II contains a conserved β3-strand Ala-Xxx-Lys sequence and domain III contains a conserved glutamate in the αC-helix that forms a salt bridge with the conserved β3-lysine in all active protein kinases (Fig. 1A) as well as many dormant protein kinase conformations (Fig. 1E). Domain V contains a three-residue hinge and four-residue linker that together connect the small lobe to the large carboxyterminal lobe.

Protein kinase domain VIB within the carboxyterminal lobe contains a conserved HRD sequence, which forms the initial portion of the catalytic loop HRD(x)$_4$N (Table 1). Domain VII contains an invariant DFG signature and domain VIII generally contains an APE-like sequence. The DFG occurs at the beginning while the APE occurs at the end of the activation segment. The activation segments, which are about 25 residues long, exhibit different conformations in the active and dormant states. Domains IX–XI make up the αE–αI helices. The X-ray crystallographic structure of the catalytic subunit of murine protein kinase A (PKA) generated a valuable blueprint for expressing the roles of the 12 Hanks domains and this structure has illuminated the fundamental biochemistry of the entire protein kinase superfamily (PDB ID: 2cpk) [10,11].

All functional protein kinases possess a small amino-terminal and a large carboxyterminal lobe that are connected by the hinge-linker segment (Fig. 1) [1,2]. The N-terminal lobe of all protein kinases contains five β-strands (β1–5) and an important regulatory αC-helix and the C-terminal lobe of active enzymes contains eight conserved helices (αD–αI and αEF1/2) along with four β-strands (β6–β9). Of the thousands

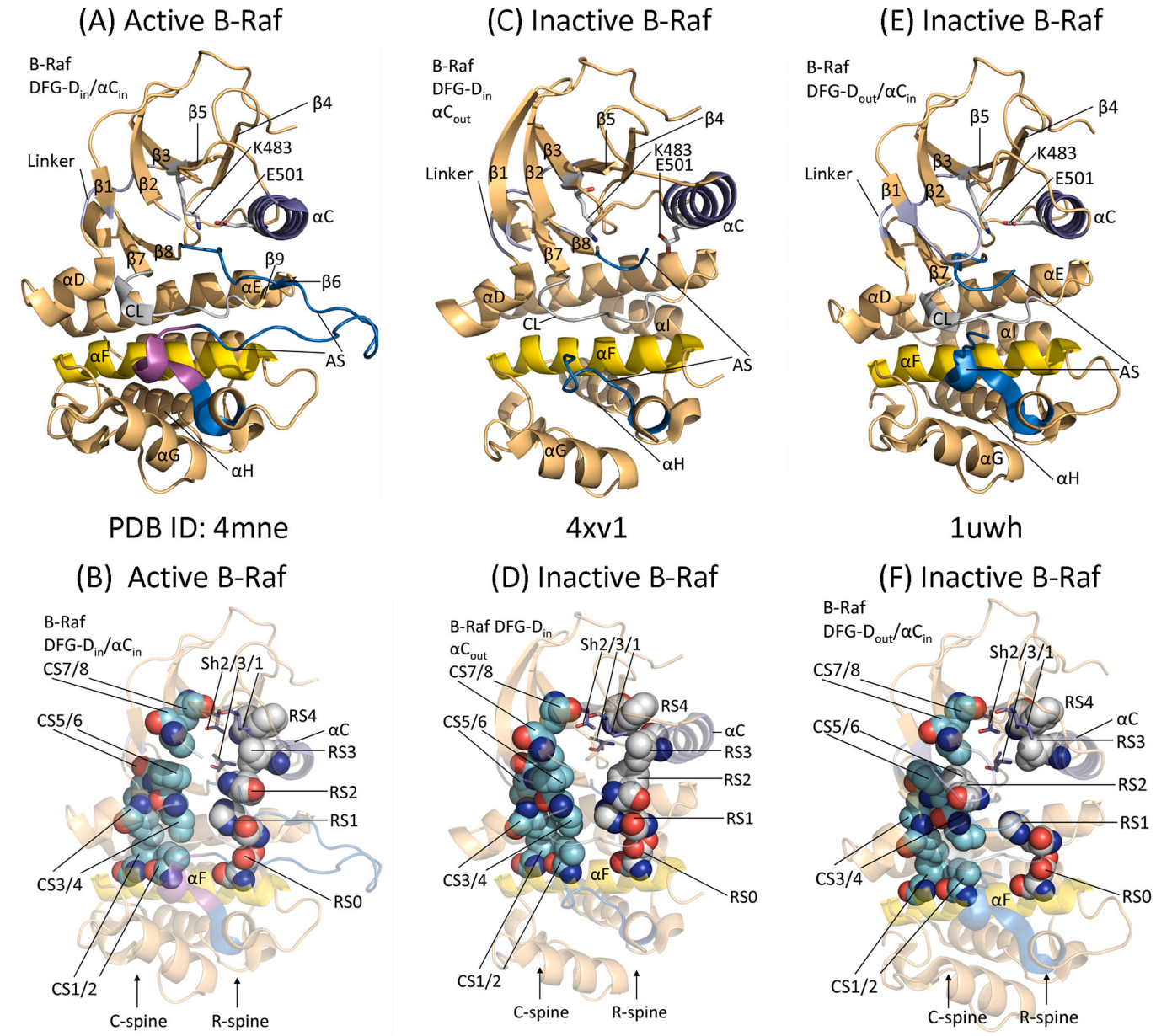

Fig. 1. (A) and (B) Active B-Raf with DFG-D$_{in}$ and αC$_{in}$. (C) and (D) Inactive B-Raf with DFG-D$_{in}$ and αC$_{out}$. (E) and (F) Inactive B-Raf with DFG-D$_{out}$ and αC$_{in}$. AS, activation segment; CL, catalytic loop; CS, catalytic spine; RS, regulatory spine. All figures except for 3–6 were prepared using the PyMOL Molecular Graphics System Version 1.5.0.4 Schrödinger, LLC.

Table 1
Important residues in selected human protein kinases[a].

	KLIFS residues	B-Raf	Abl	BTK	EGFR	MEK1	Inferred function
Component							
No. of residues	NS	766	1130	659	1210	392	
MW (kDa)	NS	84.4	122.8	76.3	134	43.4	
Protein kinase domain	NS	457–717	242–493	402–655	712–979	68–361	Catalyzes substrate phosphorylation
Glycine-rich loop	4–9	^{464}GSGSFG^{469}	^{249}GGGQYG^{254}	^{409}GTGQFG^{414}	^{719}GSGAFG^{724}	^{75}GAGNGG^{80}	Interacts with ATP/ADP adenine
β3-K, *K* of *K*/E/D/D	17	K483	K271	K430	K745	K97	Forms salt bridges with ATP α- and β-phosphates and with αC-E
αC-E, *E* of K/*E*/D/D	24	E501	E286	E445	E768	E114	Forms salt bridges with β3-K
Gatekeeper	45	T529	T315	T474	T790	M143	Regulates access to back cleft
Hinge	46–48	^{530}QWC^{532}	^{316}EFM^{318}	^{475}EYM^{477}	^{791}LMP^{793}	^{144}EHM^{146}	Connects N- and C-lobes
Linker	49–52	^{533}EGSS^{536}	^{319}TYGN^{322}	^{478}ANGC^{481}	^{794}PFGC^{797}	^{147}DGGS^{150}	
Catalytic loop	68–75	^{574}HRDLKSNN^{581}	^{361}HRDLAARN^{368}	^{519}HRDLAARN^{526}	^{835}HRDLAARN^{842}	^{188}HRDVKPSN^{195}	Plays both structural and catalytic functions
Catalytic loop HRD-D, First *D* of K/E/*D*/D	68	D576	D363	D521	D837	D190	Catalytic base
Catalytic loop Asn	75	N581	N368	N526	N842	N195	Chelates Mg^{2+}(2)
AS DFG-D, Second *D* of K/E/D/*D*	81	D594	D381	D539	D855	D208	Chelates Mg^{2+}(1)
End of AS	NS	^{621}APE^{623}	^{407}APE^{409}	^{565}PPE^{567}	^{882}ALE^{884}	^{231}SPE^{233}	Interacts with the AS-αF loop and αH-αI loop
AS phosphorylation sites	NS	T599, S602	Y393	S551	Y869	S218, S222	Stabilizes enzyme after phosphorylation
C-terminal tail	NS	718–766	494–1130	656–659	980–1210	362–392	Signal transduction
UniProtKB accession no.	NS	P15056	P00519	Q06187	P00533	Q02750	

[a] AS, activation segment; MW, molecular weight; NS, not specified.

of protein kinase structures that have been solved, all of these enzymes contain the protein kinase fold as first described for PKA [1,10,11]. Moreover, phosphatidylinositol 3-kinases, which are classified as atypical protein kinases (aPKs), have the protein kinase fold [12].

All functional protein kinases possess a Lys/Glu/Asp/Asp (K/E/D/D) amino acid signature that is required for catalysis (Table 1) [1]. The lysine and glutamate occur within the small lobe and the two aspartate residues occur within the large lobe. ATP binds next to the hinge within the cleft between the two lobes and it interacts with each lobe. Comprehensive analyses indicate that a salt bridge between the αC-glutamate and the β3-lysine is required for the formation of an active protein kinase conformation, which corresponds to an "αC_{in}" arrangement as shown for active B-Raf (Fig. 1A). These residues fail to form this salt bridge in many dormant enzymes (Fig. 1C) and thereby form an inactive "αC_{out}" structure (See Ref. [1] for details). The αC_{in} conformation is necessary, but not sufficient, for the expression of catalytic activity.

Domain VIb of the C-terminal lobe contains catalytic loop residues that play essential structural and catalytic roles. Additionally, two Mg^{2+} ions participate in each catalytic cycle of most, but not all, protein kinases [13–15]. By inference, the DFG-D594 (the second *D* of K/E/D/*D*) binds to Mg^{2+}(1), which in turn binds to the ATP β- and γ-phosphates. The asparagine residue at the end of the catalytic loop (HRD(x)$_4$N) binds to Mg^{2+}(2) with high affinity while Mg^{2+}(1) binds with lower affinity. The two Mg^{2+} ions offset the negative charges of the phosphate groups. While Mg^{2+}(1) appears to be critical for the phosphoryl transfer, Mg^{2+}(2) binds first as a complex with ATP [15]. In the active conformation, the DFG-D is directed inward toward the active site (DFG-D_{in}) where it can bind Mg^{2+}(1). In contrast, when the DFG-D is pointed outward, the resulting DFG-D_{out} structure is catalytically impaired owing to the blockade of ATP and protein substrate binding.

The protein kinase activation segment, which is 20–30 residues in length with an average length of 23 residues [16], plays an important role during catalysis [17]. DFG-F at the beginning of the segment interacts with the αC-helix above and the conserved HRD-H of the catalytic loop below. These components interact hydrophobically and form part of a regulatory spine as described later. For most eukaryotic protein kinases, the phosphorylation of one or two residues within the activation segment promotes the conversion of a dormant enzyme to a catalytically competent enzyme [18,19]. The Raf enzyme family contains two phosphorylatable residues within the activation segment (Table 1). Moreover, Zhang and Guan discovered that B-Raf activation requires the phosphorylation of activation segment T598 and S601 [20], which correspond to UniProtKB residues T599 and S602.

The HRD(x)$_4$N-D catalytic-loop aspartate, which is the first D of the K/E/*D*/D signature, functions as a Lowry-Brønsted base and removes a proton from the protein-substrate –OH group thereby facilitating the nucleophilic attack of the oxygen atom onto the γ-phosphorus atom of ATP (Fig. 2) [21]. The activation segment, when it is in its open and functional conformation, helps to position the protein substrate. The β3-lysine forms salt bridges with αC-helix glutamate and the α- and β-phosphates of ATP. Mg^{2+}(1) and DFG-D bind to the β- and γ-phosphates while Mg^{2+}(2) and β3-lysine bind to the α- and β-phosphates of ATP thereby aiding catalysis [1,14].

Kornev et al. examined the structures of 23 protein kinases and they discovered the role of several essential residues by using a local spatial pattern alignment algorithm [22,23]. They described and labeled four hydrophobic residues as a regulatory or R-spine and eight hydrophobic residues as a catalytic or C-spine. Both spines contain amino acid residues from both the amino-terminal and carboxyterminal lobes. The R-spine contains one residue from the regulatory αC-helix and another from the activation segment (DFG-F), both of which are key components that assume active and dormant conformations. The C-spine helps to position ATP within the active site cleft to allow catalysis and the R-spine stabilizes the catalytic loop and activation segment in a functional state. Moreover, the precise alignment of both spines is required for the assembly of an active enzyme.

For a summary of the properties of the spine and shell residues and their interactions with small molecule inhibitors of selected members of the protein kinase super family, see the following reviews: Refs. [24–26] for the EGFR family of protein-tyrosine kinases, Refs. [27–29] for the ALK pleotrophin and midkine receptor protein-tyrosine kinase, Ref. [30]

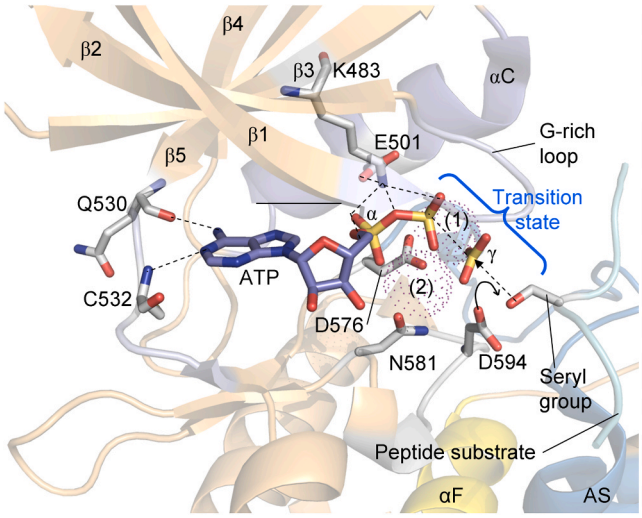

Fig. 2. Inferred mechanism and transition state of the B-Raf–catalyzed protein kinase reaction. HRD-D594 abstracts a proton from the protein-serine substrate allowing for its nucleophilic attack onto the γ-phosphorus of ATP. 1 and 2 label the two Mg^{2+} ions shown as dots. AS, activation segment. The figure was prepared from PDB IDs 3qhr and 1gy3 of CDK2, but the depicted residues are those of human B-Raf.

for the Kit stem cell receptor protein-tyrosine kinase, Ref. [31] for the fibroblast growth factor receptor family of protein-tyrosine kinases, Ref. [32] for the RET glial-cell derived receptor protein-tyrosine kinase, Ref. [33] for the PDGFRα/β protein-tyrosine kinases, Ref. [34] for the ROS1 orphan receptor protein-tyrosine kinase, Ref. [35] for the VEGFR1/2/3 protein-tyrosine kinases, Refs. [36,37] for the Src non-receptor protein-tyrosine kinase, Ref. [38] for the Janus non-receptor protein-tyrosine kinase, Refs. [39,40] for the Bruton non-receptor protein-tyrosine kinase, Refs. [6,41] for the RAF protein-serine/threonine kinases, Ref. [7,42] for the MEK1/2 dual specificity protein kinases, Refs. [43,44] for the ERK1/2 protein-serine/threonine kinases, and Refs. [45,46] for the cyclin-dependent protein-serine/threonine kinase family.

Labeling the protein kinase R-spine from the bottom to the top, it consists of the catalytic loop HRD-H (RS1), the activation loop DFG-F (RS2), an amino acid four residues C-terminal to the conserved αC-E (RS3), and a hydrophobic amino acid at the beginning of the β4-strand (RS4); RS3 is sometimes labeled αC-E+4 indicating that it is four residues C-terminal to αC-E. The HRD-H backbone N–H group forms a hydrogen bond with an invariant aspartate carboxylate group (RS0) within the αF-helix [22]. The R-spine of active protein kinases with DFG-D_{in} is linear (Fig. 1B). In contrast, the R-spine of inactive B-Raf with DFG-D_{out} is broken with a displaced RS2 residue (Fig. 1F). The R-spine of protein kinases such as B-Raf with αC_{out} results in the displacement of RS3 rightward from RS2 and RS4 (Fig. 1D). The C-spine of protein kinases contains amino acid residues from both the small and large lobes; moreover, the adenine moiety of ATP completes the C-spine [23]. The two residues of the small lobe that interact with the ATP adenine include an invariant valine at the beginning of the β2-strand (CS7) and a conserved alanine from the signature AxK of the β3-strand (CS8). Furthermore, a residue from the β7-strand (CS6) on the floor of the adenine pocket interacts hydrophobically with the adenine of ATP. Based upon the analysis of dozens of crystal structures, we find that essentially all steady-state ATP-competitive protein kinase antagonists interact with CS6. The CS6 residue is found between two hydrophobic residues (CS4 and CS5) that altogether make up the β7-strand. The CS6 residue interacts with the CS3 residue that occurs near the beginning of the αD-helix of the large lobe. CS5/6/4 immediately follow the catalytic loop asparagine $(HRD(x)_4N)$ so that these residues can be easily identified within the primary structure. The CS3 and CS4 residues interact hydrophobically with CS1 and CS2 that are found within the αF-helix to complete the C-spine (Fig. 1B) [23]. The hydrophobic αF-helix, which spans the entire large lobe, anchors both the R- and C-spines. Moreover, both spines anchor the protein kinase catalytic residues in a functional state. CS7 and CS8 in the small lobe form part of the "ceiling" of the adenine-binding pocket while CS6 in the large lobe forms part of the "floor" of the adenine-binding pocket. The adenine base of ATP occurs in the space between CS5/6 and CS7/8 in Fig. 1B.

Based upon the results of site-directed mutagenesis experiments, Meharena et al. identified three shell (Sh) residues in the PKA catalytic subunit that stabilize the R-spine; they designated these residues as Sh1, Sh2, and Sh3 [47]. The Sh2 residue corresponds to the so-called gatekeeper residue of protein kinases. The gatekeeper residue controls the access to the back cleft [48–50]. In contrast to the identification of the HRD, DFG, or APE signatures, which is based upon the primary structure [51], the two spines were identified by their spatial locations in active or inactive protein kinases [22,23]. Table 2 provides a list of the spine and shell residues of selected human enzymes considered in this review. Small molecule protein kinase antagonists often interact with residues within the C-spine as well as with R-spine and shell residues [52].

2. Classification of protein kinase-drug complexes

Dar and Shokat defined three classes of small molecule protein kinase inhibitors and named them as types I, II, and III [49]. The type I antagonists form hydrogen bonds with the protein kinase hinge and they bind within the adenine pocket of what we consider to be an active enzyme. The type II inhibitors also occupy the adenine pocket and they bind to an inactive protein kinase with the activation segment DFG-D pointing away from the active site (DFG-D_{out}). Type III inhibitors are allosteric inhibitors that block enzyme activity without displacing ATP. Zuccotto subsequently defined type I½ inhibitors as drugs that bind to an inactive protein kinase with the DFG-D pointed inward (DFG-D_{in}) toward the active site [51]. The dormant enzyme may display an $\alpha C\text{-helix}_{out}$ conformation, a closed activation segment, a nonlinear or broken regulatory spine, a DFG-D_{in} inactive conformation, or other structural features that render them inactive.

Gavrin and Saiah subsequently divided allosteric inhibitors into two types: III and IV [53]. The type III antagonists bind within the cleft between the amino-terminal and carboxyterminal lobes and next to, but independent of, the ATP binding site, while type IV allosteric inhibitors bind elsewhere. Moreover, Lamba and Ghosh defined bivalent inhibitors as those antagonists that span two distinct parts of the protein kinase domain as type V inhibitors [54]. For example, an antagonist that bound to the adenine-binding site as well as the peptide substrate site would be classified as a type V inhibitor. To complete this classification, we named compounds that bind covalently with the target enzyme as type VI antagonists [52]. For example, afatinib is a targeted covalent inhibitor (TCI) of EGFR that is FDA-approved for the treatment of NSCLC. Mechanistically, this drug binds initially and reversibly to an active EGFR conformation (like a type I inhibitor) and then the thiol group of EGFR C797 attacks the drug to form an irreversible covalent adduct [52].

We divided type I½ and type II antagonists into A and B subtypes [52]. Type A inhibitors are compounds that extend past the Sh2 gatekeeper residue into the back cleft. In contrast, type B inhibitors are agents that fail to extend into the back cleft. Based upon preliminary findings, the possible significance of this difference is that type A antagonists bind to their target enzyme with longer residence times [55] as compared with type B antagonists [52]. Sorafenib is a type IIA VEGFR2 inhibitor that is FDA approved for the treatment of renal cell carcinomas. Sunitinib is a type IIB VEGFR2 antagonist that is also FDA approved for the treatment of renal cell carcinomas. The type IIA antagonist has a residence time greater than 64 min while that of the type IIB antagonist has a residence time of less than 2.9 min [56]. Additionally, sorafenib is a type IIA inhibitor of B-Raf and CDK8 and its

Table 2
Spine and shell residues of selected human protein kinases[a].

	Spine & shell no.	KLIFS No.	B-Raf	EGFR	Abl	MEK1	BTK
Regulatory spine							
β4-strand (N-lobe)	RS4	38	F516	L777	L301	F129	L460
C-helix (N-lobe)	RS3	28	L505	M766	M290	L118	M449
Activation loop DFG-F (C-lobe)	RS2	82	F595	F856	F382	F209	F540
Catalytic loop HRD-H (C-lobe)	RS1	68	H574	H835	H361	H184	H519
F-helix (C-lobe)	RS0	None	D638	D896	D421	D245	D579
R-shell							
Two residues upstream from the gatekeeper	Sh3	43	I527	L788	I313	I141	I472
Gatekeeper, end of β5-strand	Sh2	45	T529	T790	T315	M143	T474
αC-β4 loop	Sh1	36	V511	C775	V299	V127	V458
Catalytic spine							
β3-AxK-A (N-lobe)	CS8	15	A481	A743	A269	A95	A428
β2-strand (N-lobe)	CS7	11	V471	V726	V256	V82	V416
β7-strand (C-lobe)	CS6	77	F583	L844	L370	L197	L528
β7-strand (C-lobe)	CS5	78	L584	V845	C369	V198	V529
β7-strand (C-lobe)	CS4	76	I582	V843	V371	I196	C527
D-helix (C-lobe)	CS3	53	L537	L798	M343	L151	L482
F-helix (C-lobe)	CS2	None	L649	L907	L428	S252	L586
F-helix (C-lobe)	CS1	None	V645	T903	I432	M256	I590

[a] From klifs.net.

residence times are 568 and 576 min, respectively [57].

Type II inhibitors bind to their target protein kinase with the DFG-D directed away from the active site [1,53,58] and they are usually the easiest to identify by inspection. Consequently, the DFG-D and DFG-F switch places and the change in location of the phenylalanine residue leaves a large allosteric site that interacts with a portion of type II antagonists such as sorafenib. Many type II protein kinase inhibitors form hydrogen bonds with the DFG-D backbone amide and the αC-E carboxylate.

Modi and Dunbrack performed a comprehensive analysis of the interaction of ligands with active and inactive conformations of protein kinases based upon the structure of the activation loop, which begins with the DFG signature [59]. This signature motif is observed in two major classes of conformations: DFG-D_{in} and DFG-D_{out}. In the first case the phenylalanine residue is in contact with the αC-helix of the small lobe and in the second case phenylalanine occupies the ATP site exposing an αC-helix pocket. They developed a clustering of protein kinase conformations based on the location of the phenylalanine side chain (DFG-D_{in}, DFG-D_{out}, and DFG-D_{inter} or intermediate) and the backbone dihedral angles of the xDF sequence, where x is the residue before the DFG motif. They identified eight distinct conformations and labeled them based on the Ramachandran regions (A, alpha; B, beta; L, left) of the xDF motif and χ1 refers to the phenylalanine rotamer (minus, plus, trans). Their clustering divides the DFG-D_{in} group into six groups including BLAminus, which contains active structures, and two common inactive forms, BLBplus and ABAminus. DFG_{out} structures are predominantly in the BBAminus conformation. The inactive conformations have specific features that make them unable to bind ATP, magnesium, and/or their protein substrates. These investigators produced an invaluable and non-commercial web site (http://dunbrack3.fccc.edu/kincore/) that enables one to determine the whether the protein kinase conformations correspond to an active enzyme (DFG-D_{in}, BLAminus) or an inactive enzyme (DFG-D_{in}, BLBplus, DFG-D_{in}, ABAminus, DFG-D_{out}, BBAminus). We used this web site to determine whether the conformation of the various protein kinases of the drug-enzyme complexes that we are considering are active (DFG-D_{in}, BLAminus) or inactive (otherwise). Table 3 provides a summary of the BRIMR classification scheme and a comparison with the Modi-Dunbrack scheme.

Table 3
Comparison of the BRIMR and Modi-Dunbrack FCCC inhibitor classifications[a].

BRIMR inhibitor type	BRIMR inhibitor criteria[b]	Modi-Dunbrack inhibitor types that correspond to the BRIMR inhibitor type in column 1	Modi-Dunbrack inhibitor criteria[c]
I	Binds in and around the ATP-binding pocket of an active DFG-D_{in} enzyme.	Type I (BLAminus) DFG-D_{in}	Type I – binds only to the ATP binding region with either DFG-$D_{in/out}$
I½ A	Extends into the back cleft of a DFG-D_{in} inactive enzyme.	Type I (BLBplus); type I½ back (BLBplus); type I½ back (BLBminus) DFG-D_{in}	Type I½ – binds to the ATP binding region and extends into the back pocket
I½ B	Does not extend into the back cleft of a DFG-D_{in} inactive enzyme.	Type I (BLBplus, ABAminus, BLBtrans) DFG-D_{in},	(subdivided as Type I½-front and Type I½-back depending on the contact with N-terminal or C-terminal residues of the αC-helix, respectively)
II A	Extends into the back cleft of a DFG-D_{out} enzyme.	Type II (BBAminus) DFG-D_{out}	Type II – binds to the ATP binding region and extends into the back pocket or the Type II-only region
II B	Does not extend into the back cleft of a DFG-D_{out} enzyme.	Type I DFG-D_{out}	
III	Allosteric inhibitor bound next to the ATP-binding site.	Type III, corresponds to the BRIMR classification	Type III – binds only in the back pocket without displacing ATP
IV	Allosteric inhibitor bound away from the ATP-binding site.	Allosteric, corresponds to type IV of the BRIMR classification	Allosteric – binds to any pocket outside the ATP-binding region
V	Bivalent inhibitor spanning two kinase domain regions.	Undefined	
VI	Targeted covalent inhibitor.	Undefined	

[a] BRIMR, Blue Ridge Institute for Medical Research; FCCC, Fox Chase Cancer Center.
[b] From Ref. [52].
[c] From Ref. [80].

3. Drug-ligand binding pockets

We followed the examples provided by Liao [60], van Linden et al. [61], and Kanev et al. [62] in describing and characterizing drug-binding pockets. An overview illustrating the location of the

several pockets and sub-pockets is depicted in Fig. 3 and the location of key residues making up the various sub-pockets is described in Table 4. The region between the protein kinase small and large lobes is divided into a front cleft or front pocket, a gate area, and a back cleft. The back pocket or hydrophobic pocket II (HPII) contains the gate area and the adjoining back cleft. The front cleft includes the glycine-rich loop, the hinge residues, the adenine pocket, the linker connecting the hinge residues to the large lobe αD-helix, the αD-helix, and the amino acid residues within the catalytic loop (HRD(x)$_4$N). The gate area includes a portion of the β3-strand, part of the β3-strand–αC-helix loop of the small lobe, and the proximal portion of the activation segment of the large lobe. The back cleft includes the αC-β4 back loop, the αC-helix, portions of the β4- and β5-strands of the small lobe and a section of the αE-helix within the large lobe. The location of the KLIFS residues is given in Fig. 4.

Van Linden et al. [61] and Kanev et al. [62] identified several sub-pockets that are found in these three regions [60]. For example, the front cleft includes an adenine-binding pocket (AP) adjacent to two front pockets named FP-I and FP-II. FP-I occurs between the catalytic loop HRD(x)$_4$N-asparagine and the xDFG-motif (where x is the residue immediately before the activation segment DFG). FP-II is found against the glycine-rich loop and the β3-strand at the top of the cleft. Back pocket I (BP-I) can be divided into two sub-pockets. BP-I-A occurs between the conserved β3-K of the AxK signature and the β5-strand and gatekeeper residue. BP-I-B is found between DFG and the β3- and β5-strands. BP-I-A and BP-I-B occur in the DFG-D$_{in}$ and DFG-D$_{out}$ conformations (Fig. 3).

BP-II-A-in and BP-II-in occur within the back cleft in the DFG-D$_{in}$ conformation [60]. BP-II-A-in occurs between the distal αC-helix, the back loop, and DFG-F. BP-II-B-in is found between the αC-glutamate, the distal portion of the αC-helix, the β4-strand, and DFG-F. Major changes of BP-II-A-in and BP-II-in take place to produce BP-II-out that is found only in the DFG-D$_{out}$ configuration; this conversion is centered on a change in the location of DFG-F. The resulting compartment is found where the DFG-F residue occurs in the DFG-D$_{in}$ conformation and is named back pocket II-out (BP-II-out). This pocket is bordered by the middle of the αC-helix, the proximal back loop, the distal back loop, the αE-helix, the β6-strand, and HRD-H. Back pocket III (BP-III) is also found only in the DFG-D$_{out}$ conformation. This compartment is bordered by the back loop and the β8-strand. BP-IV and BP-V are two pockets that are partially solvent exposed. BP-IV extends from the β6-strand to HRD-H on one side and the αC-helix RS3 residue on the other side. BP-V is found beneath the αC-helix in the DFG-D$_{out}$ conformation. See Table 4 for a list of the KLIFS residues that make up these sub-pockets.

Table 4
Location of KLIFS sub-pockets.

Sub-pocket	KLIFS residues[a]	Description[b]
FP-I	75, 79–82	Between DFG and HRD(x)$_4$N-N of the CL of DFG-D$_{in/out}$
FP-II	4–10	Near the open GRL conformation of DFG-D$_{in/out}$
BP-I-A	16–17, 43–45	Found in the upper gate area against/between the β-3 and β-5 sheets of DFG-D$_{in/out}$
BP-I-B	16–17, 28, 43,81– 82	Between DFG and the β-3 and β-5 sheets of DFG-D$_{in/out}$
BP-II-in	24, 28, 35–38, 82	Between DFG, the αC-helix, and the back loop of DFG-D$_{in}$
BP-II-A-in	28, 35–38, 82	Between DFG, the back loop, and the β-4 sheet of DFG-D$_{in}$
BP-II-B	24, 28, 38, 82	Near DFG-F, αC-E, and the proximal β-4 strand of DFG-D$_{in/out}$
BP-II-out	27, 31, 35, 61, 66, 68	Near the distal αC-helix, the back loop, and above the HRD-H of DFG-D$_{out}$
BP-III	31, 35, 79	Near the back loop and DFG-D minus 2 of DFG-D$_{out}$
BP-IV	27, 66–68	Deep in the back pocket near the distal αC-helix and HRD of DFG-D$_{out}$
BP-V	20, 23, 24, 27	Beneath αC-E and the middle of the αC-helix of DFG-D$_{out}$

[a] klifs.net.
[b] CL, catalytic loop; GRL, glycine-rich loop.

Kanev et al. formulated a comprehensive summary of ligand and drug binding to more than 5200 human and mouse protein kinase domains [62]. Their KLIFS (kinase–ligand interaction fingerprint and structure) catalog includes an alignment of 85 ligand binding-site residues occurring in both the small and large lobes; this information facilitates the comparison and classification of drugs and ligands based upon their binding interactions and expedites the detection of related and unique interactions. Furthermore, these investigators devised a standard amino acid residue numbering system that aids in the comparison of multiple protein kinases. Table 2 specifies the relationship between the KLIFS database numbering and the catalytic spine, shell, and regulatory spine amino acid residue nomenclature. Moreover, this consortium established a valuable non-commercial and searchable web site that is regularly updated and provides comprehensive information on the interaction of ligands and drugs with ePKs and aPKs (klifs.net).

Carles et al. created another web-based resource providing a list of ePK and aPK inhibitors that have been approved or that are in clinical trials [63]. Their non-commercial and searchable web site is updated

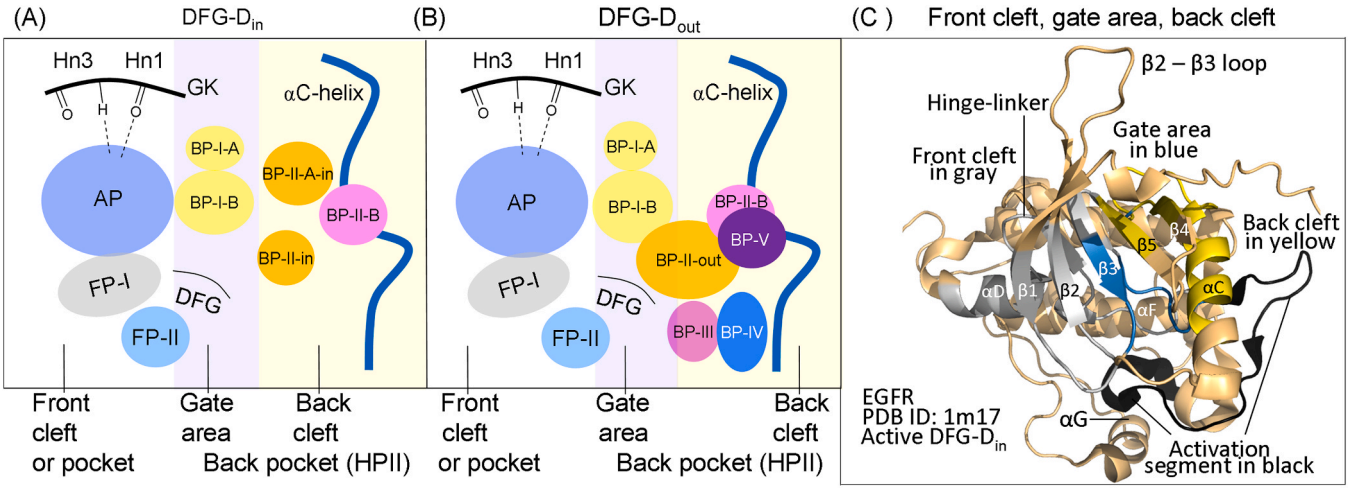

Fig. 3. Location of the protein kinase domain drug-binding pockets in the (A) DFG-D$_{in}$ and (B) DFG-D$_{out}$ conformations. (C) Location of the front cleft, gate area, and back cleft in EGFR. AP, adenine pocket; BP, back pocket; FP, front pocket; GK, gatekeeper; Hn, hinge; HPII, hydrophobic pocket II.
Adapted from Refs [60–62].

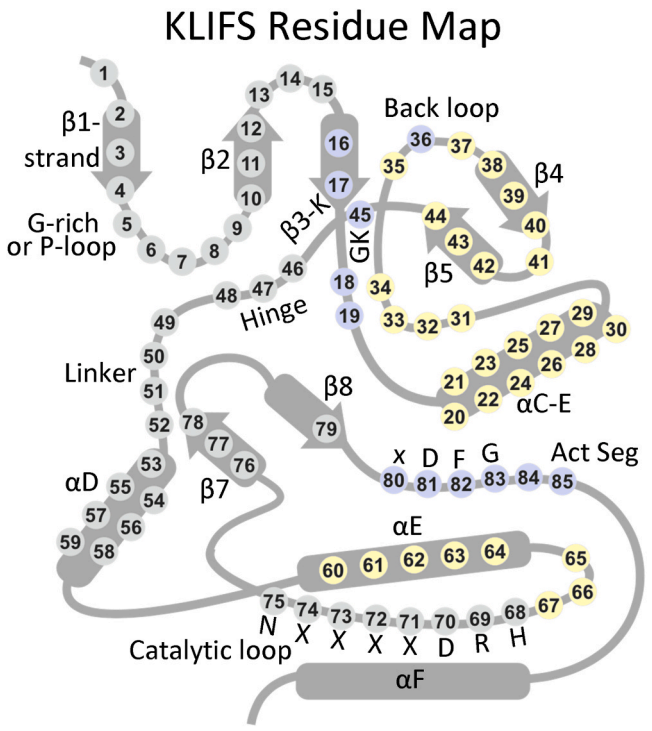

Fig. 4. The location of KLIFS residues within a generic protein kinase domain. Act Seg, activation segment; GK, gatekeeper. Front cleft residues have a gray background; gate area residues, blue; back cleft, yellow. Template provided by Dr. Albert J. Kooistra.

regularly and depicts the structure of the various antagonists, their protein kinase targets, therapeutic indications, physical properties, year of first approval (if applicable), and their trade name (http://www.icoa.fr/pkidb/). Similarly, the Blue Ridge Institute for Medical Research maintains a web site that lists the FDA-approved ePK inhibitors and portrays their (i) structures, (ii) number of hydrogen bond donors, (iii) number of hydrogen bond acceptors, (iv) the calculated $\log_{10}$ of the distribution coefficient, (v) the number of rings and rotatable bonds, (vi) the year of initial approval, (vii) primary protein kinase targets, and (viii) therapeutic indications. The site also provides a link to the corresponding US FDA labels that describe the therapeutic indications and usage, dosage, warnings and precautions, adverse reactions, and clinical pharmacology. This web site, which is found at www.brimr.org/PKI/PKIs.htm, is regularly updated.

4. Drug-enzyme interactions

Our previous reviews and updates listed the poses of the FDA-approved drugs with their targets with an emphasis on the hydrophobic interactions with the spine and shell residues [12,39,64,65]. Fig. 5 provides a summary of the hydrophobic interactions of FDA-approved drugs with their presumed therapeutic targets (the interaction of FDA-approved drugs with protein kinases that are not thought to be therapeutic targets, which amount to about two dozen X-ray crystal structures, are not listed). The first row in the figure gives a breakdown of the regions of ePKs beginning with the β1-strand, glycine-rich loop, β2-strand, and so forth. The next row depicts significant structural residues such as CS7, CS8, the β3-strand lysine, and so on. The third row labels the KLIFS residues from 1 through 85 that interact with approved drugs and other ligands. The fourth row indicates residues that belong to the front cleft (gray), the gate area (light blue), and the back cleft (yellow). The first section depicts the interaction of ADP with the aurora protein-serine/threonine kinase A (AurkA). The following sectional rows correspond to the type I, type I½A, type I½B, type IIA, type IIB, type III, and finally type VI inhibitors according to the BRIMR scheme [52]. A black Greek ϕ denotes a pure hydrophobic interaction between the enzyme and the drug; a blue ϕ denotes a hydrophobic and hydrogen bond donor interaction emanating from the enzyme; a red ϕ symbolizes a hydrophobic, hydrogen bond donor, and hydrogen bond acceptor interaction between the enzyme and drug; a green ϕ denotes a hydrophobic and hydrogen bond acceptor interaction emanating from the enzyme; A indicates that the enzyme residue functions as a hydrogen bond acceptor; B denotes that the enzyme residue functions as both a hydrogen bond donor and acceptor; and D indicates that the enzyme residue functions as a hydrogen bond donor.

We now consider the pose of prototypical drugs with their target enzymes beginning with the gefitinib-EGFR complex (PDB ID: 2ity). Gefitinib is an anilino-quinazoline derivative (Fig. 6A) that is approved for the treatment of *EGFR* mutation-positive NSCLC [66,67]. The drug inhibits EGFR with IC_{50} values in the subnanomolar range; it has activity against several other protein kinases, but the IC_{50} values are in the micromolar range (klifs.net). Based upon the analysis of Modi and Dunbrack (dunbrack3.fccc.edu/kincore/), the enzyme has the active BLAminus structure and we therefore classify gefitinib as a type I EGFR inhibitor. The X-ray crystal structure with EGFR demonstrates that the *N*1 quinazoline forms a hydrogen bond with the backbone amide of M793 (Fig. 7A). The drug makes hydrophobic contact with four spine residues (RS3, CS6/7/8) and two shell residues (Sh2/3) including the T790 gatekeeper. The KLIFS analysis indicates that the quinazoline occurs in the adenine pocket and the anilino group occurs in the gate area (BP-I-A, BP-I-B). All residues with which gefitinib (depicted as a line structure) makes hydrophobic contacts are shown as sticks; those with gray carbon atoms reside in the front cleft (F) and those with the blue carbon atoms are in the gate area (G) as shown in Fig. 7B. All KLIFS residues with which gefitinib interacts are indicated in Fig. 5 (see supplementary material).

Vemurafenib is a pyrrolo[2,3-*b*]pyridine derivative (Fig. 6B) that is used in the treatment of Erdheim-Chester disease and advanced $BRAF^{V600E}$-mutant melanoma [68,69]. The IC_{50} values of vemurafenib for the mutant are two orders of magnitude greater than that for A-Raf or B-Raf (klifs.net). This has the therapeutic advantage of blocking the mutant enzyme at concentrations that do not hinder the physiological action of wild type A/B-Raf. Erdheim-Chester disease is characterized by non-Langerhans cell histiocytosis that exhibits xanthogranulomatous infiltrations of multiple organs by lipid-laden histiocytes. The pathogenesis of this rare malady is unclear. Based upon the analysis of Modi and Dunbrack, the enzyme has the inactive BLAplus structure (dunbrack3.fccc.edu/kincore/) and it extends into the back cleft and we therefore classify this as a type I½A inhibitor. The X-ray crystal structure of vemurafenib with B-Raf shows that the pyrrolo moiety forms a hydrogen bond with the carbonyl oxygen of Q530 (the first hinge residue) and the *N*1 pyridine forms a hydrogen bond with the backbone N–H group of C532 (the third hinge residue). Additionally, one of the sulfonamide oxygen atoms forms hydrogen bonds with the N–H groups of both DFG-F595 and DFG-G596 (Fig. 7C). The drug makes hydrophobic contact with six spine residues (RS2/3/4, CS6/7/8) and two shell residues (Sh2/3). The KLIFS analysis indicates that the pyrrolopyridine occurs within the adenine pocket and the 2,4-difluorophenyl propane-1-sulfonamide occupies the gate area (BP-I-A, BP-I-B) and the back cleft (BP-II-in and BP-II-A-in). All residues with which vemurafenib (depicted as a line structure) makes hydrophobic contacts are shown as sticks; those with gray carbon atoms reside in the front cleft (F), those with the blue carbon atoms are in the gate area (G), and those with yellow carbon atoms are found within the back cleft (B) as depicted in Fig. 7D. All KLIFS residues with which vemurafenib interacts are shown in Fig. 5. B-Raf exists in an inactive αC_{out} configuration with DFG-D_{in} and the overall classification of the B-Raf–vemurafenib complex conforms to that of a type I½A antagonist [52].

Imatinib is a 2-amino-4-pyrido-pyrimidine derivative (Fig. 6C) that is FDA-approved for the treatment of Philadelphia chromosome-positive

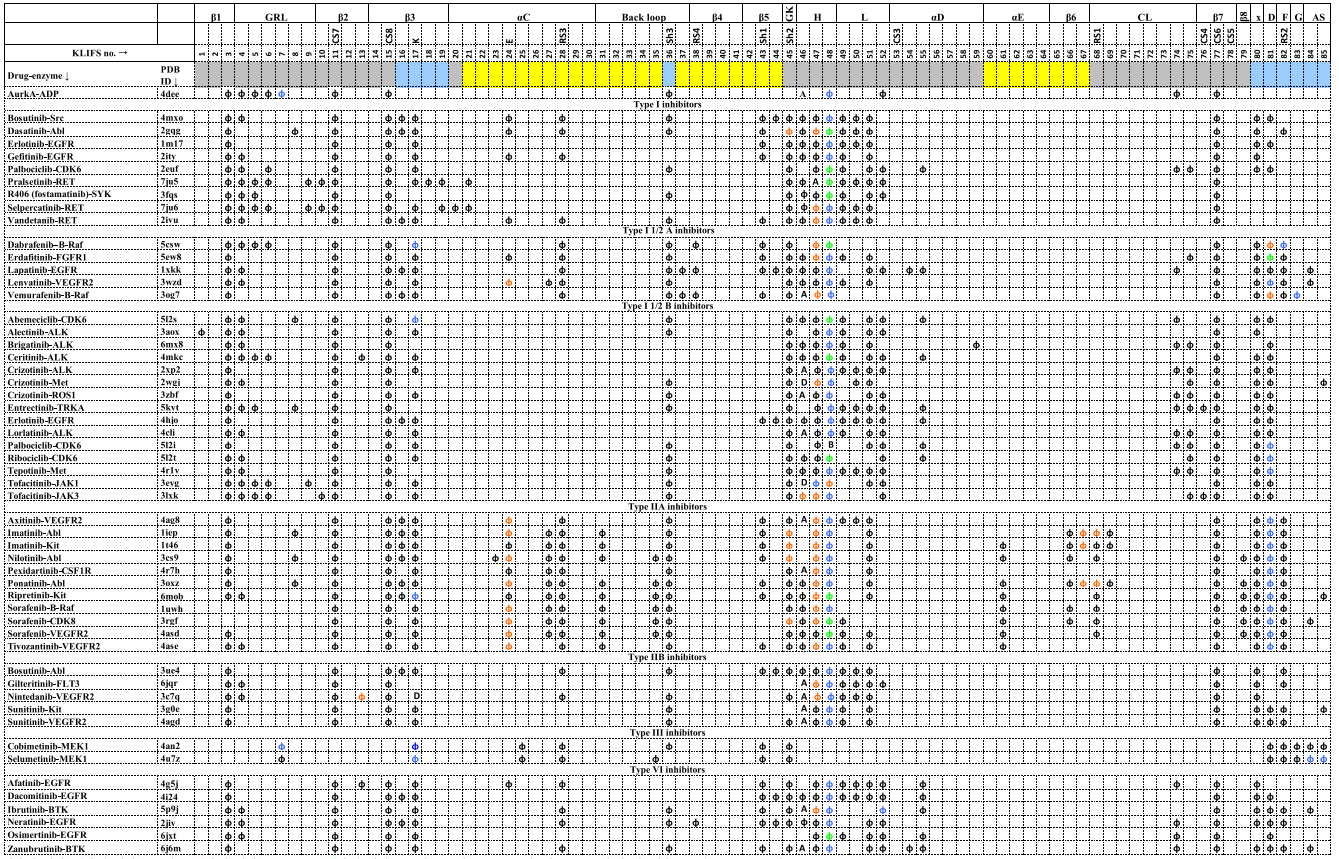

Fig. 5. Interaction of selected FDA-approved small molecule protein kinase inhibitors with their target enzymes using the KLIFS standard nomenclature. A black ϕ indicates a hydrophobic interaction; a blue ϕ indicates that the enzyme residue interacts hydrophobically with the drug and functions as a hydrogen bond donor; a red ϕ indicates that the enzyme residue interacts with the drug hydrophobically and functions as a hydrogen bond acceptor; a green ϕ indicates that the enzyme residue interacts hydrophobically with the drug and functions as both a hydrogen bond donor and acceptor; A indicates that the enzyme residue functions as a hydrogen bond acceptor; D indicates that the enzyme residue functions as a hydrogen bond donor, and B indicates that the enzyme residue functions as both a hydrogen bond donor and acceptor. Curated data derived from klifs.net.

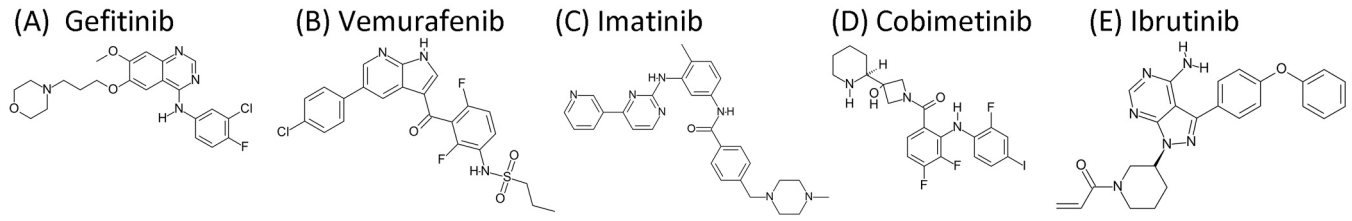

Fig. 6. Structures of selected small molecule protein kinase inhibitors.

chronic myelogenous leukemias, Kit mutation-positive gastrointestinal stromal tumors, hypereosinophilic syndrome, chronic eosinophilic leukemias, dermatofibrosarcoma protuberans, myelodysplastic/myeloproliferative diseases with *PDGFR* gene-rearrangements, aggressive systemic mastocytosis without the *KIT* ^{D816V} mutation, and acute lymphoblastic leukemias [1,30,41,43,44,70,71]. The drug is a multikinase inhibitor with activity against Abl, Abl2, PDGFRα/β, and Kit (klifs.net). Based upon the analysis of Modi and Dunbrack (dunbrack3.fccc.edu/kincore/), the enzyme has the inactive DFG-D_{out}-BBAminus structure and it extends into the back cleft and we therefore classify this as a type IIA inhibitor. The X-ray crystal structure of imatinib bound to Abl shows that the pyridine *N*1 forms a hydrogen bond with the N–H group of M318 (the third hinge residue) and the amino group forms a hydrogen bond with the hydroxyl group of the gatekeeper T315. Furthermore, the benzamide oxygen forms a polar bond with the N–H group of DFG-D381 and the benzamide N–H group forms a hydrogen bond with the αC-E286. The piperazine *N*4 forms polar bonds with the carbonyl groups of I360 and HRD-H361 (Fig. 7E). The drug makes hydrophobic contact with six spine residues (RS2/3/4, CS6/7/8) and all three shell residues. The amino-pyrimidine-pyridine moiety is found in the adenine pocket and the remainder of the drug occupies the gate area (BP-I-A, BP-I-B), BP-II-out, and BP-IV. The drug binds to dormant Abl with DFG-D_{out} and it extends into the back pocket; these properties are those of a type IIA inhibitor [52]. All residues with which imatinib (depicted as a line structure) makes hydrophobic contacts are shown as sticks; those with gray carbon atoms reside in the front cleft, those with the blue carbon atoms are in the gate area, and those with yellow carbon atoms are found within the back cleft (Fig. 7F). All KLIFS residues with which imatinib interacts are shown in Fig. 5. Abl exists in an inactive DFG-D_{out} and αC_{out} configuration and the overall classification of this complex conforms to that of a type IIA antagonist [52]. The approval of imatinib for the treatment of chronic myelogenous leukemias in 2001 paved the way for the discovery and development of all small molecule protein kinase inhibitors [1].

Cobimetinib is an anilino-benzene derivative (Fig. 6D) that is approved as a first-line treatment of *BRAF*^{V600E}-mutant melanomas in combination with vemurafenib [72–75]. Its inhibitory potency against other protein kinases has not been tested (klifs.net). Cobimetinib is a

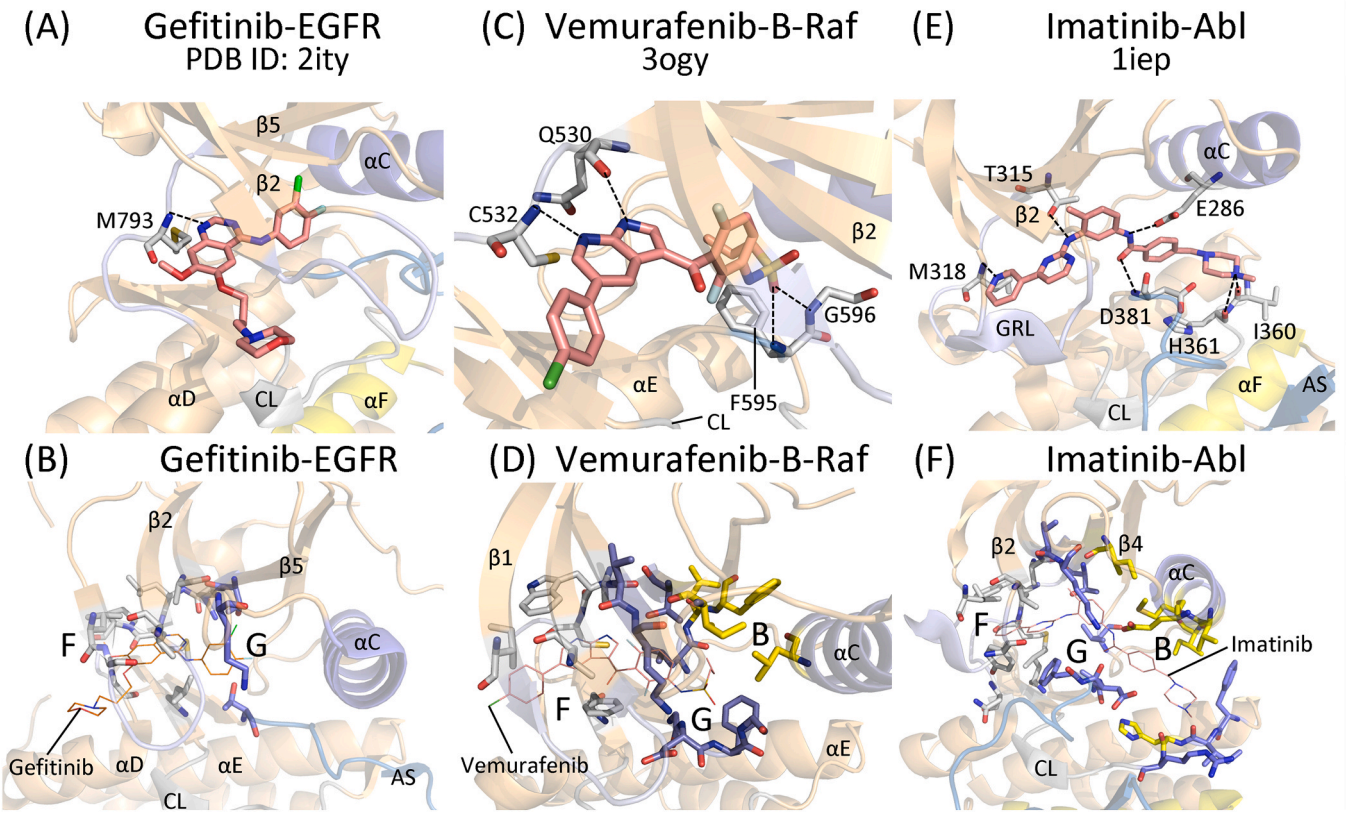

Fig. 7. (A) Polar interaction of gefitinib with EGFR is indicated by the dashed line. (B) Gefitinib-EGFR hydrophobic interactions. (C) Polar interactions of vemurafenib with B-Raf are shown by the dashed lines. (D) Vemurafenib-B-Raf hydrophobic interactions. (E) Polar interactions of imatinib with Abl are shown by the dashed lines. (F) Imatinib-Abl hydrophobic interactions. In (B), (D), and (F), the drugs are shown as lines with orange carbon atoms and the letters F, G, and B in the figures refer to the front cleft residues with gray carbon atoms, gate area residues with blue carbon atoms and back cleft residues with yellow carbon atoms, respectively. CL, catalytic loop.

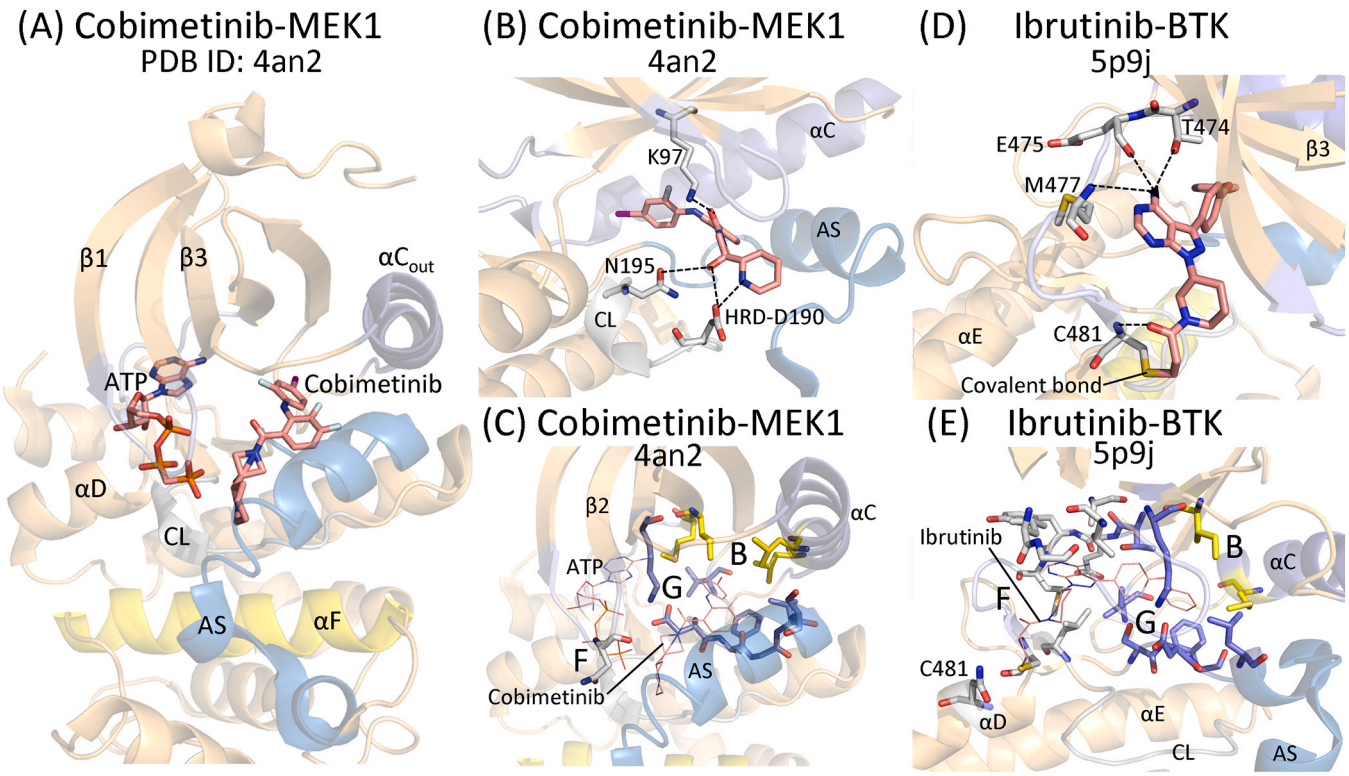

Fig. 8. (A) The structure of cobimetinib and an ATP analog (β, γ-methylene adenosine 5′-triphosphate, AMP-PCP) bound to MEK1. (B) Polar interactions of cobimetinib with MEK1 are shown by the dashed lines. (C) Cobimetinib-MEK1 hydrophobic interactions. (D) Polar interactions of ibrutinib with BTK are shown by the dashed lines. (E) Ibrutinib-BTK hydrophobic interactions. In (C) and (E), the ATP analog and the drugs are shown as lines with orange carbon atoms. F, front cleft residues have gray carbon atoms; G, gate area residues have blue carbon atoms; B, back cleft residues have yellow carbon atoms; AS, activation segment; CL, catalytic loop.

MEK1/2 antagonist while vemurafenib is a B-Raf inhibitor as described above. Cobimetinib is a type III antagonist and Fig. 8A demonstrates that it can bind to its target along with an ATP analog (AMP-PCP). The X-ray crystal structure of cobimetanib with MEK1 shows that the 3-hydroxyl group makes hydrogen bonds with the side-chain amide nitrogen of N195 at the end of the catalytic loop and with the carboxylate group of HRD-D190. Moreover, the carbonyl oxygen makes a polar bond with AxK-K97 of the β3-strand and the piperidine *N*1 makes a hydrogen bond with the HRD-D190 carboxylate group (Fig. 8B). The drug makes hydrophobic contact with one spine residue (RS3). All residues with which cobimetinib (depicted as a line structure) makes hydrophobic contacts are shown as sticks; the one with the gray carbon atom (N78) is in the front cleft, those with the blue carbon atoms are in the gate area, and those with yellow carbon atoms are found within the back cleft (Fig. 8C). Its contacts with the KLIFS residues are enumerated in Fig. 5. The drug also makes hydrophobic contact with L215, G225, and T226 (residues lacking KLIFS numbers). The drug occurs in the front pocket and the gate area and the diarylamino group occurs in the back pocket including BP-II-in. Note that cobimetinib does not occupy the adenine pocket, but it does occur in the deep cleft between the amino-terminal and carboxyterminal lobes; it is therefore classified as a type III allosteric inhibitor [52].

Ibrutinib is an amino pyrazolo[3,4-*d*]-pyrimidine derivative (Fig. 6E) that targets BTK and is used in the treatment of chronic lymphocytic leukemias, mantle cell lymphomas, graph vs. host disease, and Waldenström macroglobulinemia [76–79]. Its inhibitory power against other protein kinases has not been examined (klifs.net). The drug is a covalent (type VI) inhibitor of Bruton tyrosine kinase. The X-ray structure with BTK shows that the 4-amino group forms a hydrogen bond with E475 (the first hinge residue) and the pyrimidine *N*3 forms a hydrogen bond with the N–H group of M477 (the third hinge residue). The drug forms a covalent Michael adduct with C481 that is found in the linker segment and the carbonyl oxygen of the drug forms a hydrogen bond with the backbone amide of the same residue (Fig. 8D). The medicinal makes hydrophobic contact with five spine residues (RS2/3, CS6/7/8) and all three shell residues. All residues with which ibrutinib (depicted as a line structure) makes hydrophobic contacts are shown as sticks; those with the gray carbon atoms are in the front cleft, those with the blue carbon atoms are in the gate area, and those with yellow carbon atoms are found within the back cleft (Fig. 8E). Its contacts with the KLIFS residues are enumerated in Fig. 5. The amino-pyrimidine occurs within the adenine pocket and the phenoxyphenyl group occupies BP-I-B within the gate area. Ibrutinib binds to an inactive enzyme with DFG-D$_{in}$, but with αC$_{out}$ as observed with type I½ antagonists. However, ibrutinib is classified as a type VI inhibitor because of the covalent nature of its inhibition [52].

The mode of interaction of the FDA-approved drugs with their targets is summarized in Fig. 5 (see supplementary material). All of these drugs with the exception of sorafenib (type IIA) and cobimetinib and selumetinib (type III) interact with the front cleft KLIFS-3 of the β3-strand. With the exception of the type III inhibitors, all of the drugs interact hydrophobically with CS6 (KLIFS-77), CS7 (KLIFS-11), CS8 (KLIFS-15, or AxK-A), AxK-K (KLIFS-17), and residues within the hinge-linker region (KLIFS-46–52); these drugs also form hydrogen bonds with the third hinge residue (KLIFS-48). The vast majority of drugs, including the type III inhibitors, interact with the gatekeeper residue (KLIFS-45). Note however that ADP does not interact with the gatekeeper. The type IIA inhibitors have the most hydrophobic interactions with their target enzymes. These include interactions with KLIFS-27/31/35/61/66, all within the back pocket. There is also considerable interaction with RS1 (KLIFS-68), the conserved HRD-H that occurs in the back pocket of type II antagonists, but within the front pocket of the other types of inhibitors.

5. Comparison of the BRIMR and Modi-Dunbrack inhibitor classifications

The distinction between active and dormant conformations of protein kinases is a key consideration in the characterization of small molecule inhibitors. DFG-$D_{in/out}$, αC-$helix_{in/out}$, and $AS_{open/closed}$ represent major conformational states [1]. The interaction, or pose, of each drug with a protein kinase target is usually, but not always, unique. It is useful to classify these poses and apply them to the drug discovery process. The classification into inhibitor types permits a discussion of the

Table 5
Blue Ridge Institute for Medical Research (BRIMR), Modi-Dunbrack Fox Chase Cancer Center (FCCC), and Kinase Ligand Interaction and Fingerprint and Structure (KLIFS) inhibitor data base comparisons.

Ligand/Drug-enzyme	PDB ID	BRIMR type[a]	FCCC type[b,c]	FCCC: Dihedral angles & DFG-D[c]	KLIFS pockets[d]
ADP-AurkA	4dee	I	I	BLAminus & DFG-D_{in}	F, FP-II
BRIMR type I inhibitors					
Bosutinib-Src	4mxo	I	I	BLAminus & DFG-D_{in}	F,G, BP-I-A/B
Dasatinib-Abl	2gqg	I	I, I½b	BLAminus & DFG-D_{in}	F, G, B, BP-I-A/B
Erlotinib-EGFR	1m17	I	I	BLAminus & DFG-D_{in}	F, G, B, BP-I-A/B
Gefitinib-EGFR	2ity	I	I	BLAminus & DFG-D_{in}	F,G, BP-I-A/B
Palbociclib-CDK6	2euf	I	I	BLAminus & DFG-D_{in}	F
Pralsetinib-RET	7ju5	I	I	BLAminus & DFG-D_{in}	F, FP-II
R406 (fostamatinib)	3fqs	I	I	BLAminus & DFG-D_{in}	F
Selpercatinib-RET	7ju6	I	I½f	BLAminus & DFG-D_{in}	F, FP-II
Vandetanib-RET	2ivu	I	I	BLAminus & DFG-D_{in}	F,G, BP-I-A/B
BRIMR type I½A inhibitors					
Dabrafenib–B-Raf	5csw	I½A	I½b	BLBminus & DFG-D_{in}	F, G, B, BP-I-A/B, BP-II-in, BP-II-A-in
Erdafitinib-FGFR1	5ew8	I½A	I½b	BLAplus & DFG-D_{in}	F, G, B, BP-I-A/B
Lapatinib-EGFR	1xkk	I½A	I½b	BLAplus & DFG-D_{in}	F, G, B, BP-I-A/B, BP-II-in, BP-II-A-in
Lenvatinib-VEGFR2	3wzd	I½A	I	BLBplus & DFG-D_{in}	F, G, B, BP-I-B, BP-II-in
Vemurafenib-B-Raf	3og7	I½A	I½b	BLAplus & DFG-D_{in}	F, G, B, FP-I, BP-I-A/B, BP-II-in, BP-II-A-in
BRIMR type I½B inhibitors					
Abemeciclib-CDK6	5l2s	I½B	I	BLBplus & DFG-D_{in}	F, FP-II
Alectinib-ALK	3aox	I½B	I	ABAminus & DFG-D_{in}	F, BP-I-B
Brigatinib-ALK	6mx8	I½B	I	ABAminus & DFG-D_{in}	F, FP-I
Ceritinib-ALK	4mkc	I½B	I	ABAminus & DFG-D_{in}	F, FP-I
Crizotinib-ALK	2xp2	I½B	I	ABAminus & DFG-D_{in}	F, FP-I
Crizotinib-Met	2wgj	I½B	I	BLBplus & DFG-D_{in}	F, FP-I
Crizotinib-ROS1	3zbf	I½B	I	ABAminus & DFG-D_{in}	F, FP-I
Entrectinib-TRKA	5kvt	I½B	I	ABAminus & DFG-D_{in}	F, FP-I
Erlotinib-EGFR	4hjo	I½B	I	BLBtrans & DFG-D_{in}	F, G, BP-I-A/B
Lorlatinib-ALK	4cli	I½B	I	ABAminus & DFG-D_{in}	F, FP-I
Palbociclib-CDK6	5l2i	I½B	I	BLBplus & DFG-D_{in}	F
Ribociclib-CDK6	5l2t	I½B	I	BLBplus & DFG-D_{in}	F, G, FP-I
Tepotinib-Met	4r1v	I½B	I	BLBplus & DFG-D_{in}	F, FP-I
Tofacitinib-JAK1	3eyg	I½B	I	ABAminus & DFG-D_{in}	F, FP-I/II
Tofacitinib-JAK3	3lxk	I½B	I	ABAminus & DFG-D_{in}	F, FP-I/II
BRIMR type IIA inhibitors					
Axitinib-VEGFR2	4ag8	IIA	I	BBAminus & DFG-D_{out}	F, G, B, BP-I-B, BP-II-out
Imatinib-Abl[e]	1iep	IIA	II	BBAminus & DFG-D_{out}	F, G, B, BP-I-A/B, BP-II-out, BP-IV
Imatinib-Kit	1t46	IIA	II	BBAminus & DFG-D_{out}	F, G, B, BP-I-A/B, BP-II-out, BP-IV
Nilotinib-Abl	3cs9	IIA	II	BBAminus & DFG-D_{out}	F, G, B, BP-I-A/B, BP-II-out, BP-V
Pexidartinib-CSF1R	4r7h	IIA	II	BBAminus & DFG-D_{out}	F, G, B, BP-I-B, BP-II-out, BP-V
Ponatinib-Abl[e]	3oxz	IIA	II	BBAminus & DFG-D_{out}	F, G, B, BP-I-A/B, BP-II-out, BP-III, BP-IV
Ripretinib-Kit	6mob	IIA	II	BBAminus & DFG-D_{out}	F, G, B, BP-I-A/B, BP-II-out, BP-III
Sorafenib-B-Raf	1uwh	IIA	II	BBAminus & DFG-D_{out}	F, G, B, BP-I-B, BP-II-out
Sorafenib-CDK8	3rgf	IIA	II	BBAminus & DFG-D_{out}	F, G, B, BP-I-B, BP-II-out, BP-III
Sorafenib-VEGFR2	4asd	IIA	II	BBAminus & DFG-D_{out}	F, G, B, BP-I-B, BP-II-out, BP-III
Tivozantinib-VEGFR2	4ase	IIA	II	BBAminus & DFG-D_{out}	F, G, B, BP-I-B, BP-II-out
BRIMR type IIB inhibitors					
Bosutinib-Abl	3ue4	IIB	I	Unassigned & DFG-D_{out}	F, G, BP-II-A/B
Gilteritinib-FLT3	6jqr	IIB	I	Unassigned & DFG-D_{out}	F
Nintedanib-VEGFR2	3c7q	IIB	I	Unassigned & DFG-D_{out}	F, G, BP-I-B
Sunitinib-Kit	3g0e	IIB	I	Unassigned & DFG-D_{out}	F
Sunitinib-VEGFR2	4agd	IIB	I	BBAminus & DFG-D_{out}	F, BP-I-B
BRIMR type III inhibitors					
Cobimetinib-MEK1	4an2	III	III, I	BLBplus & DFG-D_{in}	G, B, BP-II-in
Selumetinib-MEK1	4u7z	III	III, I	BLBplus & DFG-D_{in}	G, B, BP-II-in
BRIMR type VI inhibitors					
Afatinib-EGFR	4g5j	VI	I	BLAminus & DFG-D_{in}; allosteric	F, G, BP-I-A/B
Dacomitinib-EGFR	4i24	VI	I	BLBtrans & DFG-D_{in}	F, G, BP-I-B
Ibrutinib-BTK	5p9j	VI	I½b	BLBplus & DFG-D_{in}	F, G, B, BP-I-B
Neratinib-EGFR	2jiv	VI	I½b	BLBplus & DFG-D_{in}	F, G, B, BP-I-A/B
Osimertinib-EGFR	6jxt	VI	I	BLBtrans & DFG-D_{in}	F
Zanubrutinib-BTK	6j6m	VI	I½b	BLBplus & DFG-D_{in}	F, G, B, BP-I-B

[a] Ref. [52]
[b] b, back; f, front
[c] http://dunbrack3.fccc.edu/kincore/
[d] klifs.net
[e] Mouse enzyme

nature of drug-enzyme interactions using a few terms and not exhaustive descriptions. The BRIMR classification outlined in Table 3 is adapted from that of previous authors [49,51,53,54] with some modifications. For example, Dar and Shokat classify PP1 bound to Hck as a type I inhibitor [49]. However, the X-ray crystal structure shows that PP1 binds to the DFG-D_{in}/αC-$helix_{out}$ conformation (PDB ID: 1qcf). The drug occupies the front cleft and gate area, but not the back cleft (klifs.net); we would classify PP1 as a type I½B inhibitor because the drug is bound to a dormant enzyme and does not extend into the back cleft. Similarly, Zuccotto et al. classify sunitinib as a type I inhibitor [51]. However, it binds to (i) the protein-serine/threonine CDK2 with the DFG-D_{in} and αC-$helix_{out}$ conformation (PDB ID:3til) and it binds to (ii) the receptor protein-tyrosine kinases Kit (PDB ID: 3g0e) and VEGFR2 (PDB ID: 4agd) with the DFG-D_{out} and αC-$helix_{out}$ conformation. The drug occupies the front cleft and the gate area and does not extend to the back cleft. These correspond to type I½B and type IIB inhibitors in our classification, respectively. We and other investigators classify inhibitors bound to the DFG-D_{out} as type II inhibitors. However, Modi and Dunbrack [80] classify antagonists that bind to a DFG-D_{out} conformation but fail to extend into the back pocket as a type I inhibitor.

We consider any drug that is bound to an active protein kinase as a type I inhibitor and we use the algorithm developed by Modi and Dunbrack [59] to determine whether or not the kinase is active. According to their scheme, an active enzyme has the xDF dihedral angles and a phenylalanine rotamer notation abbreviated by BLAminus. If an enzyme has DFG-D_{in}, but is not BLAminus, we would classify it as a type I½ inhibitor. Our previous papers classified brigatinib-Alk (6mx8), crizotinib-ROS1 (3zbf), tofacitinib-JAK1 (3eyg), and tofacitinib-JAK3 (3lxk) as type I inhibitors [52,64,65]. These drug-enzyme complexes have αC_{in}, DFG-D_{in} with linear R-spines, and open activation segments and by inspection appeared to be in the active conformation. However, the Modi-Dunbrack algorithm (http://dunbrack3.fccc.edu/kincore/) classifies them as ABAminus with DFG-D_{in}, an inactive enzyme form, and we have accordingly moved them into the type I½B category (Fig. 5). We classify any inhibitor bound to a DFG-D_{out} enzyme form as a type II inhibitor. Modi and Dunbrack classify our type I½ inhibitors as type I or type I½ antagonists. Their definitions of type III and type IV inhibitors correspond closely to ours. Regardless of the nature of the enzyme conformation (usually type I or type I½), we classify targeted covalent inhibitors (TCIs) as type VI antagonists.

Modi and Dunbrack analyzed the X-ray crystal structures of more than 1300 drug-enzyme complexes and found that type I inhibitors made up of about 57% of the total number of antagonists, type I½ antagonists made up about 30%, type II inhibitors made up about 7%, and 6% were unclassifiable [59,80]. Our data on the interaction of FDA-approved inhibitors with their target enzymes indicates that type I inhibitors make up only 9% of the drug-enzyme complexes, type I½ inhibitors make up 20%, type II inhibitors make up 16%, and 6% correspond to type VI covalent inhibitors (Table 5). These data indicate that there is a significant increase in the percentage of type II inhibitors and significant decrease in the percentage of the type I inhibitors in the FDA-approved category when compared with all of the available drug-protein kinase X-ray crystal structures in the public domain. However, the percentage comparisons are approximations owing to the different classification criteria used in this review and those of Modi and Dunbrack (Table 3).

That a given antagonist can bind to different conformations of its targets adds to the complexity of inhibitor classification schemes [52]. Bosutinib is a type I inhibitor of Src and a type IIB inhibitor of Abl, both of which are protein-tyrosine kinases. Erlotinib is a type I and I½B inhibitor of EGFR, a receptor protein-tyrosine kinase. Additionally, palbociclib is a type I and I½B inhibitor of CDK6, a protein-serine/threonine kinase. These results demonstrate that small molecule protein kinase antagonists are not necessarily conformationally selective. Moreover, these data indicate that medicinals that occupy only the adenine pocket and gate area may be interchangeable as type I and I½B antagonists.

We followed the suggestion of Gavrin and Saiah and subdivided the allosteric inhibitors into two categories (Table 3) [53]. The type III antagonists bind to an allosteric site next to the adenine-binding pocket whereas the type IV antagonists bind elsewhere. Lamba and Ghosh classified type V antagonists as those that bind to two different portions of the kinase fold [54]. Parang et al. described a type V ATP-analog peptide conjugate bound to the insulin receptor protein-tyrosine kinase domain that extends from the ATP-binding pocket to the peptide/protein substrate binding site [81]. All of these inhibitors are readily reversible. Targeted covalent inhibitors generally bind irreversibly and whether they are classified as irreversible inhibitors, other, or type VI inhibitors is arbitrary.

The era of targeting protein kinases for therapeutic purposes is but two decades old and is therefore in its early stages. Thus far only about three dozen protein kinases represent bona fide drug targets [65] out of a family consisting of more than 500 enzymes [82] and one can expect that the number of targets will increase. The FDA is approving small molecule protein kinase inhibitors at a rate of three or more per year and there is no sign that this will abate. Most of the current therapeutic indications are for neoplastic diseases including lymphomas, leukemias, and various carcinomas. The approval of tofacitinib and upadacitinib for the treatment of rheumatoid arthritis, nintedanib for idiopathic pulmonary fibrosis, netarsudil for glaucoma, and fedratinib for myelofibrosis represents an expanded therapeutic repertoire that we anticipate will increase in the future. Neoplasms and malignancies are characterized by genome instability and the development of resistance to both targeted and cytotoxic therapies [1]. Whether inflammatory and non-neoplastic disorders will display similar secondary resistance to targeted therapies remains to be established.

Owing to the participation of protein kinase signaling cascades in a wide variety of physiological and pathological processes, one can foresee the extended use of targeted inhibitors both as primary and secondary treatments for many additional illnesses. We can expect the use of targeted protein kinase inhibitors as agents for the treatment, inter alia, of ankylosing spondylitis, atopic dermatitis, asthma, diabetes, hypertension, lupus erythematosus, papilloma, Parkinson disease, plaque psoriasis, and pulmonary hypertension [83–85]. Further studies of protein kinase structure and signal transduction pathways promises to yield new and actionable information that will serve as a basis for fundamental and applied biomedical breakthroughs.

Conflict of interest

The author is unaware of any affiliations, memberships, or financial holdings that might be perceived as affecting the objectivity of this review.

Acknowledgements

I thank Dr. Albert J. Kooistra for providing the template depicted in Fig. 4 and for sharing his insight on the properties of the various protein kinase binding sub-pockets listed in Table 4. I thank Laura M. Roskoski for providing editorial and bibliographic assistance. I also acknowledge the assistance of Jasper Martinsek and Josie Rudnicki for their help in preparing the figures and W.S. Sheppard and Pasha Brezina for their help in structural analyses. The colored figures in this paper were evaluated to ensure that their perception was accurately conveyed to colorblind readers [86].

Appendix A. Supplementary data

Supplementary material related to this article can be found, in the online version, at doi:10.1016/j.phrs.2021.105660.

References

[1] R. Roskoski Jr., A historical overview of protein kinases and their targeted small molecule inhibitors, Pharmacol. Res. 100 (2015) 1–23.
[2] P.A. Schwartz, B.W. Murray, Protein kinase biochemistry and drug discovery, Bioorg. Chem. 39 (2011) 192–210.
[3] D. Fabbro, S.W. Cowan-Jacob, H. Moebitz, Ten things you should know about protein kinases: IUPHAR review 14, Br. J. Pharmacol. 172 (2015) 2675–2700.
[4] A.J. Kooistra, A. Volkamer, Kinase-centric computational drug development, Ann. Rep. Med. Chem. 50 (2017) 197–236.
[5] G. Manning, D.B. Whyte, R. Martinez, T. Hunter, S. Sudarsanam, The protein kinase complement of the human genome, Science 298 (2002) 1912–1934.
[6] R. Roskoski Jr., RAF protein-serine/threonine kinases: structure and regulation, Biochem. Biophys. Res. Commun. 399 (2010) 313–317.
[7] R. Roskoski Jr., MEK1/2 dual-specificity protein kinases: structure and regulation, Biochem. Biophys. Res. Commun. 417 (2012) 5–10.
[8] V. Modi, R.L. Dunbrack Jr., A structurally-validated multiple sequence alignment of 497 human protein kinase domains, Sci. Rep. 9 (2019) 19790.
[9] S.K. Hanks, T. Hunter, Protein kinases 6. The eukaryotic protein kinase superfamily: kinase (catalytic) domain structure and classification, FASEB J. 9 (1995) 576–596.
[10] D.R. Knighton, J.H. Zheng, L.F. Ten Eyck, V.A. Ashford, N.H. Xuong, S.S. Taylor, J. M. Sowadski, Crystal structure of the catalytic subunit of cyclic adenosine monophosphate-dependent protein kinase, Science 253 (1991) 407–414.
[11] D.R. Knighton, J.H. Zheng, L.F. Ten Eyck, N.H. Xuong, S.S. Taylor, J.M. Sowadski, Structure of a peptide inhibitor bound to the catalytic subunit of cyclic adenosine monophosphate-dependent protein kinase, Science 253 (1991) 414–420.
[12] R. Roskoski Jr., Properties of FDA-approved small molecule phosphatidylinositol 3-kinase inhibitors prescribed for the treatment of malignancies, Pharmacol. Res. 168 (2021), 105579.
[13] R. Roskoski Jr., Src protein-tyrosine kinase structure, mechanism, and small molecule inhibitors, Pharmacol. Res. 94 (2015) 9–25.
[14] A.C. Bastidas, M.S. Deal, J.M. Steichen, Y. Guo, J. Wu, S.S. Taylor, Phosphoryl transfer by protein kinase A is captured in a crystal lattice, J. Am. Chem. Soc. 135 (2013) 4788–4798.
[15] M.J. Knape, F.W. Herberg, Metal coordination in kinases and pseudokinases, Biochem. Soc. Trans. 45 (2017) 653–663.
[16] A. Haldane, W.F. Flynn, P. He, R.M. Levy, Coevolutionary landscape of kinase family proteins: sequence probabilities and functional motifs, Biophys. J. 114 (2018) 21–31.
[17] S.S. Taylor, M.M. Keshwani, J.M. Steichen, A.P. Kornev, Evolution of the eukaryotic protein kinases as dynamic molecular switches, Philos. Trans. R. Soc. Lond. B Biol. Sci. 367 (2012) 2517–2528.
[18] B. Nolen, S. Taylor, G. Ghosh, Regulation of protein kinases; controlling activity through activation segment conformation, Mol. Cell 15 (2004) 661–675.
[19] D.J. Rawlings, A.M. Scharenberg, H. Park, M.I. Wahl, S. Lin, R.M. Kato, A. C. Fluckiger, O.N. Witte, J.P. Kinet, Activation of BTK by a phosphorylation mechanism initiated by SRC family kinases, Science 271 (1996) 822–825.
[20] B.H. Zhang, K.L. Guan, Activation of B-Raf kinase requires phosphorylation of the conserved residues Thr598 and Ser601, EMBO J. 19 (2000) 5429–5439.
[21] J. Zhou, J.A. Adams, Participation of ADP dissociation in the rate-determining step in cAMP-dependent protein kinase, Biochemistry 36 (1997) 15733–15738.
[22] A.P. Kornev, N.M. Haste, S.S. Taylor, Ten, L.F. Eyck, Surface comparison of active and inactive protein kinases identifies a conserved activation mechanism, Proc. Natl. Acad. Sci. USA 103 (2006) 17783–17788.
[23] A.P. Kornev, S.S. Taylor, Ten, L.F. Eyck, A helix scaffold for the assembly of active protein kinases, Proc. Natl. Acad. Sci. USA 105 (2008) 14377–14382.
[24] R. Roskoski Jr., The ErbB/HER family of protein-tyrosine kinases and cancer, Pharmacol. Res. 79 (2014) 34–74.
[25] R. Roskoski Jr., ErbB/HER protein-tyrosine kinases: structure and small molecule inhibitors, Pharmacol. Res. 87 (2014) 42–59.
[26] R. Roskoski Jr., Small molecule inhibitors targeting the EGFR/ErbB family of protein-tyrosine kinases in human cancers, Pharmacol. Res. 139 (2019) 395–411.
[27] R. Roskoski Jr., Anaplastic lymphoma kinase (ALK) inhibitors in the treatment of ALK-driven lung cancers, Pharmacol. Res 117 (2017) 343–356.
[28] R. Roskoski Jr., The preclinical profile of crizotinib in the treatment of non-small cell lung cancer and other neoplastic disorders, Expert Opin. Drug Dis. 8 (2013) 1165–1179.
[29] R. Roskoski Jr., Anaplastic lymphoma kinase (ALK): structure, oncogenic activation, and pharmacological inhibition, Pharmacol. Res. 68 (2013) 68–94.
[30] R. Roskoski Jr., The role of small molecule Kit protein-tyrosine kinase inhibitors in the treatment of neoplastic disorders, Pharmacol. Res. 133 (2018) 35–52.
[31] R. Roskoski Jr., The role of fibroblast growth factor receptor (FGFR) protein-tyrosine kinase inhibitors in the treatment of cancers including those of the urinary bladder, Pharmacol. Res. 151 (2020), 104567.
[32] R. Roskoski Jr., A. Sadeghi-Nejad, Role of RET protein-tyrosine kinase inhibitors in the treatment RET-driven thyroid and lung cancers, Pharmacol. Res. 128 (2018) 1–17.
[33] R. Roskoski Jr., The role of small molecule platelet-derived growth factor receptor (PDGFR) inhibitors in the treatment of neoplastic disorders, Pharmacol. Res. 129 (2018) 65–83.
[34] R. Roskoski Jr., ROS1 protein-tyrosine kinase inhibitors in the treatment of ROS1 fusion protein-driven non-small cell lung cancers, Pharmacol. Res. 121 (2017) 202–212.
[35] R. Roskoski Jr., Vascular endothelial growth factor (VEGF) and VEGF receptor inhibitors in the treatment of renal cell carcinomas, Pharmacol. Res. 120 (2017) 116–132.
[36] R. Roskoski Jr., Src protein-tyrosine kinase structure, mechanism, and small molecule inhibitors, Pharmacol. Res. 94 (2015) 9–25.
[37] M.C. Frame, R. Roskoski Jr., Src family tyrosine kinases. Reference Module in Life Sciences, Elsevier, Amsterdam, 2017, pp. 1–11, https://doi.org/10.1016/B978-0-12-809633-8.07199-5.
[38] R. Roskoski Jr., Janus kinase (JAK) inhibitors in the treatment of inflammatory and neoplastic diseases, Pharmacol. Res. 111 (2016) 784–803.
[39] R. Roskoski Jr. Orally effective FDA-approved protein kinase targeted covalent inhibitors (TCIs). Pharmacol Res. 2021 ⟨https://doi.org/10.1016/j.phrs.2021.105422⟩.
[40] R. Roskoski Jr., Ibrutinib inhibition of Bruton protein-tyrosine kinase (BTK) in the treatment of B cell neoplasms, Pharmacol. Res. 113 (2016) 395–408.
[41] R. Roskoski Jr., Targeting oncogenic Raf protein-serine/threonine kinases in human cancers, Pharmacol. Res. 135 (2018) 239–258.
[42] R. Roskoski Jr., Allosteric MEK1/2 inhibitors including cobimetanib and trametinib in the treatment of cutaneous melanomas, Pharmacol. Res. 117 (2017) 20–31.
[43] R. Roskoski Jr., ERK1/2 MAP kinases: structure, function, and regulation, Pharmacol. Res. 66 (2012) 105–143.
[44] R. Roskoski Jr., Targeting ERK1/2 protein-serine/threonine kinases in human cancers, Pharmacol. Res. 142 (2019) 151–168.
[45] R. Roskoski Jr., Cyclin-dependent protein serine/threonine kinase inhibitors as anticancer drugs, Pharmacol. Res. 139 (2019) 471–488.
[46] R. Roskoski Jr., Cyclin-dependent protein kinase inhibitors including palbociclib as anticancer drugs, Pharmacol. Res. 111 (2016) 784–803.
[47] H.S. Meharena, P. Chang, M.M. Keshwani, K. Oruganty, A.K. Nene, N. Kannan, S. S. Taylor, A.P. Kornev, Deciphering the structural basis of eukaryotic protein kinase regulation, PLoS Biol. 11 (2013), 1001680.
[48] Y. Liu, K. Shah, F. Yang, L. Witucki, K.M. Shokat, A molecular gate which controls unnatural ATP analogue recognition by the tyrosine kinase v-Src. Bioorg. Med. Chem. 6 (1998) 1219–1226.
[49] A.C. Dar, K.M. Shokat, The evolution of protein kinase inhibitors from antagonists to agonists of cellular signaling, Annu. Rev. Biochem. 80 (2011) 769–795.
[50] P.M. Ung, R. Rahman, A. Schlessinger, Redefining the protein kinase conformational space with machine learning, Cell Chem. Biol. 25 (2018) (916-24. e2).
[51] F. Zuccotto, E. Ardini, E. Casale, M. Angiolini, Through the "gatekeeper door": exploiting the active kinase conformation, J. Med. Chem. 53 (2010) 2691–2694.
[52] R. Roskoski Jr., Classification of small molecule protein kinase inhibitors based upon the structures of their drug-enzyme complexes, Pharmacol. Res. 103 (2016) 26–48.
[53] L.K. Gavrin, E. Saiah, Approaches to discover non-ATP site kinase inhibitors, Med. Chem. Commun. 4 (2013) 41–51.
[54] V. Lamba, I. Ghosh, New directions in targeting protein kinases: focusing upon true allosteric and bivalent inhibitors, Curr. Pharm. Des. 18 (2012) 2936–2945.
[55] R.A. Copeland, The drug-target residence time model: a 10-year retrospective, Nat. Rev. Drug Discov. 15 (2016) 87–95.
[56] K. Okamoto, M. Ikemori-Kawada, A. Jestel, K. von König, Y. Funahashi, T. Matsushima, A. Tsuruoka, A. Inoue, J. Matsui, Distinct binding mode of multikinase inhibitor lenvatinib revealed by biochemical characterization, ACS Med. Chem. Lett. 6 (2014) 89–94.
[57] L. Neumann, K. von König, D. Ullmann, HTS reporter displacement assay for fragment screening and fragment evolution toward leads with optimized binding kinetics, binding selectivity, and thermodynamic signature, Methods Enzym. 493 (2011) 299–320.
[58] D. Bajusz, G.G. Ferenczy, G.M. Keserá, Structure-based virtual screening approaches in kinase-directed drug discovery, Curr. Top. Med. Chem. 17 (2017) 2235–2259.
[59] V. Modi, R.L. Dunbrack Jr., Defining a new nomenclature for the structures of active and inactive kinases, Proc. Natl. Acad. Sci. USA 116 (2019) 6818–6827.
[60] J.J. Liao, Molecular recognition of protein kinase binding pockets for design of potent and selective kinase inhibitors, J. Med. Chem. 50 (2007) 409–424.
[61] O.P. van Linden, A.J. Kooistra, R. Leurs, I.J. de Esch, C. de Graaf, KLIFS: a knowledge-based structural database to navigate kinase-ligand interaction space, J. Med. Chem. 57 (2014) 249–277.
[62] G.K. Kanev, C. de Graaf, B.A. Westerman, I.J.P. de Esch, A.J. Kooistra, KLIFS: an overhaul after the first 5 years of supporting kinase research, Nucleic Acids Res 49 (2021) D562–D569.
[63] F. Carles, S. Bourg, C. Meyer, P. Bonnet, PKIDB: a curated, annotated and updated database of protein kinase inhibitors in clinical trials, Molecules 23 (4) (2018), https://doi.org/10.3390/molecules23040908 (pii: E908).
[64] R. Roskoski Jr., Properties of FDA-approved small molecule protein kinase inhibitors: a 2020 update, Pharmacol. Res. 152 (2020), 104609.
[65] R. Roskoski Jr., Properties of FDA-approved small molecule protein kinase inhibitors: a 2021 update, Pharmacol. Res. 165 (2021), 105463.
[66] D. Kazandjian, G.M. Blumenthal, W. Yuan, K. He, P. Keegan, R. Pazdur, FDA approval of gefitinib for the treatment of patients with metastatic *EGFR* mutation-positive non-small cell lung cancer, Clin. Cancer Res. 22 (2016) 1307–1312.
[67] C.R. Kucharczuk, A. Ganetsky, J.M. Vozniak, Drug-drug interactions, safety, and pharmacokinetics of EGFR tyrosine kinase inhibitors for the treatment of non-small cell lung cancer, J. Adv. Pr. Oncol. 9 (2018) 189–200.
[68] C. Garbe, T.K. Eigentler, Vemurafenib, Recent Results Cancer Res. 211 (2018) 77–89.

[69] F. Haroun, K. Millado, I. Tabbara, Erdheim-Chester disease: comprehensive review of molecular profiling and therapeutic advances, Anticancer Res. 37 (2017) 2777–2783.
[70] P.M. Fischer, Approved and experimental small-molecule oncology kinase inhibitor drugs: a mid-2016 overview, Med. Res. Rev. 37 (2017) 314–367.
[71] F. Rossari, F. Minutolo, E. Orciuolo, Past, present, and future of Bcr-Abl inhibitors: from chemical development to clinical efficacy, J. Hematol. Oncol. 11 (2018) 84.
[72] S. Kakadia, N. Yarlagadda, R. Awad, M. Kundranda, J. Niu, B. Naraev, L. Mina, T. Dragovich, M. Gimbel, F. Mahmoud, Mechanisms of resistance to BRAF and MEK inhibitors and clinical update of US Food and Drug Administration-approved targeted therapy in advanced melanoma, OncoTargets Ther. 11 (2018) 7095–7107.
[73] K.P. Garnock-Jones, Cobimetinib: first global approval, Drugs 75 (2015) 1823–1830.
[74] J. Signorelli, A. Shah Gandhi, Cobimetinib, Ann. Pharmacother. 51 (2017) 146–153.
[75] G.M. Keating, Cobimetinib plus vemurafenib: a review in $BRAF^{V600}$ mutation-positive unresectable or metastatic melanoma, Drugs 76 (2016) 605–615.
[76] D. Miklos, C.S. Cutler, M. Arora, E.K. Waller, M. Jagasia, I. Pusic, M.E. Flowers, A. C. Logan, R. Nakamura, B.R. Blazar, Y. Li, S. Chang, I. Lal, J. Dubovsky, D.F. James, L. Styles, S. Jaglowski, Ibrutinib for chronic graft-versus-host disease after failure of prior therapy, Blood 130 (2017) 2243–2250.
[77] M.A. Spinner, G. Varma, R.H. Advani, Novel approaches in Waldenström macroglobulinemia, Hematol. Oncol. Clin. North Am. 32 (2018) 875–890.
[78] P. Strati, N. Jain, S. O'Brien, Chronic lymphocytic leukemia: diagnosis and treatment, Mayo Clin. Proc. 93 (2018) 651–664.
[79] S. Pal Singh, F. Dammeijer, R.W. Hendriks, Role of Bruton's tyrosine kinase in B cells and malignancies, Mol. Cancer 17 (2018) 57.
[80] Modi V., Dunbrack RL Jr. Kincore: a web resource for structural classification of protein kinases and their inhibitors. ⟨https://doi.org/10.1101/2021.02.12.430923⟩.
[81] K. Parang, J.H. Till, A.J. Ablooglu, R.A. Kohanski, S.R. Hubbard, P.A. Cole, Mechanism-based design of a protein kinase inhibitor, Nat. Struct. Biol. 8 (2001) 31–41.
[82] G.K. Kanev, C. de Graaf, I.J.P. de Esch, R. Leurs, T. Würdinger, B.A. Westerman, A. J. Kooistra, The landscape of atypical and eukaryotic protein kinases, Trends Pharmacol. Sci. 40 (2019) 818–832.
[83] P. Cohen, D.R. Alessi, Kinase drug discovery—what's next in the field? ACS Chem. Biol. 8 (2013) 96–104.
[84] A. Levitzki, Tyrosine kinase inhibitors: views of selectivity, sensitivity, and clinical performance, Annu. Rev. Pharmacol. Toxicol. 53 (2013) 161–185.
[85] Z. Xie, X. Yang, Y. Duan, J. Han, C. Liao, Small-molecule kinase inhibitors for the treatment of nononcologic diseases, J. Med. Chem. 64 (2021) 1283–1345.
[86] R. Roskoski Jr., Guidelines for preparing color figures for everyone including the colorblind, Pharmacol. Res. 119 (2017) 240–241 (Erratum in: Pharmacol Res 2019;139:569).